Holography: analysis of convolution algorithms to reconstruct images from digital holograms

Pascal PICART
Patrice TANKAM

09.03.2024

Table des matières

I.Présentation

Module :

Holography: analysis of convolution algorithms to reconstruct images from digital holograms

Auteur(s) :

Pascal Picart & Patrice Tankam - Le Mans Université

Résumé :

The course discusses convolution algorithms to reconstruct off-axis digital holograms. The problem of convolution is addressed by considering the spatial spectral properties of digital holograms, especially the unusual localization property of the Fourier spectrum of the hologram, in regard to the physical object space. After deriving the sampling requirements for the transfer functions, three approaches are considered with the concept of spatial bandwidth extension: zero-padding, spectrum scanning and adjustable magnification. The theoretical discussion is completed by experimental illustrations that enable the algorithms to be objectively compared.

Mots-clés :

Holography, convolution algorithms, digital holograms

Pré-requis :

-

Objectif(s) pédagogique(s) :

-

Plan du cours :

- Introduction
- Theoretical basics
- Related reconstruction algorithms
- Experimental demonstration
- Conclusion

Conception & production :

Le Mans Université

Licence :

1 - http://www.gnu.org/licenses/fdl.txt

II.Cours

For a few years, digital holography [1 [Direct recording of holograms by a CCD target and numerical reconstruction], 2 [Methods of digital holography: a comparison], 3 [Phase-shifting digital holography]] has become a very stimulating topic for the scientific community working in this area. The main motivations are related to the reconstruction of objects or micro-objects in true colors [4 [Phase shifting color digital holography], 5 [Recording and reconstruction of a color holographic image by using digital lensless Fourier transform holography], 6 [Parallel phase-shifting color digital holography using two phase shifts], 7 [Parallel phase-shifting digital holography capable of simultaneously capturing visible and invisible three-dimensional information], 8 [Color lensless digital holographic microscopy with micrometer resolution]]. Yamaguchi proposed the first demonstration of the applicability of digital holography to encode and decode color objects [4 [Phase shifting color digital holography]]. Since then, several applications have been proposed in contactless measurements, such as weak flow analysis [9 [Dynamic digital holographic interferometry with three wavelengths],10 [Digital three-color holographic interferometry for flow analysis]], surface shape [11 [Pulsed digital holography for high-speed contouring that uses a two-wavelength method], 12 [Direct shape measurement by digital wave front reconstruction and multi-wavelength contouring], 13 [Surface shape measurement by phase-shifting digital holography with a wavelength shift], 14 [Multiple-wavelength digital holographic interferometry using tunable laser diodes], 15 [Large step-height measurements using multiple-wavelength holographic interferometry with tunable laser diodes], 16 [Microscopic TV holography for MEMS deflection and 3-D surface profile characterization], 17 [Real-time dual-wavelength digital holographic microscopy with a single hologram acquisition]] and multidimensional deformation measurements [18 [Method of digital holographic recording and reconstruction using a stacked color image sensor], 19 [Real-time three-sensitivity measurements based on three-color digital Fresnel holographic interferometry], 20 [Use of digital color holography for crack investigation in electronic components]], and phase contrast imaging [21 [Quantitative phase imaging by three-wavelength digital holography]-22 [Phase imaging of cells by simultaneous dual wavelength reflection digital holography]].

Different approaches to record and reconstruct holograms were discussed in the past, including the imaging specific properties of digital holography [1 [Direct recording of holograms by a CCD target and numerical reconstruction], 2 [Methods of digital holography: a comparison]-23 [Frequency analysis of digital holography], 24 [Frequency analysis of digital holography with reconstruction by convolution], 25 [Effect of the fill factor of CCD pixels on digital holograms: comment on the paper], 26 [Image formation in phase shifting digital holography and application to microscopy], 27 [Complex-wave retrieval from a single off-axis hologram], 28 [Imaging analysis of digital holography], 29 [General theoretical formulation of image formation in digital Fresnel holography], 30 [Off-axis digital hologram reconstruction: some practical considerations], 31 [Parallel two-step phase-shifting digital holography]]. The reconstructions of the amplitude and the phase of the encoded object are based on the numerical simulation of the light diffracted through the numerical aperture (digital hologram) [1 [Direct recording of holograms by a CCD target and numerical reconstruction]]. The algorithms have the same theoretical background [32 [Introduction to Fourier Optics]]; although their implementation may depend on the recording scheme, i.e., in-line holography [33 [Diffraction from a wavelet point of view], 34 [Image reconstruction for in-line holography with the Yang-Gu algorithm], 35 [Reconstruction of in-line digital holograms from two intensity measurements], 36 [Digital in-line holographic microscopy]], off-axis Fresnel holography [1 [Direct recording of holograms by a CCD target and numerical reconstruction], 2 [Methods of digital holography: a comparison], 3 [Phase-shifting digital holography]], digital Fourier holography [28 [Imaging analysis of digital holography], 29 [General theoretical formulation of image formation in digital Fresnel holography], 30 [Off-axis digital hologram reconstruction: some practical considerations], 31 [Parallel two-step phase-shifting digital holography], 32 [Introduction to Fourier Optics], 33 [Diffraction from a wavelet point of view], 34 [Image

reconstruction for in-line holography with the Yang-Gu algorithm], 35 [Reconstruction of in-line digital holograms from two intensity measurements], 36 [Digital in-line holographic microscopy], 37 [Digital recording and numerical reconstruction of lens less Fourier holograms in optical metrology]], and reconstruction with Fresnelets in off-axis holography [27 [Complex-wave retrieval from a single off-axis hologram]].

One can distinguish two main ways to reconstruct the encoded objects: the first is based on diffraction formulation in the Fresnel approximation [32 [Introduction to Fourier Optics]], leading to the two-dimensional discrete Fresnel transform [1 [Direct recording of holograms by a CCD target and numerical reconstruction],2 [Methods of digital holography: a comparison]], whereas the second consists in the convolution approach of the diffraction [2 [Methods of digital holography: a comparison], 24 [Frequency analysis of digital holography with reconstruction by convolution],38 [Wavelength-scanning digital interference holography for tomographic three-dimensional imaging by use of the angular spectrum method], 39 [Fast algorithms for free-space diffraction patterns calculation], 40] [Diffraction transfer function and its calculation of classic diffraction formula]. The latter requires considering some particular sampling constraints [39 [Fast algorithms for free-space diffraction patterns calculation]]. This course aims at discussing such particular spectral properties of digital off-axis holograms. It especially focuses on a convolution approach that is quite adapted to the reconstruction of digital color holograms.

The course is organized as follows : Sections 2 presents the theoretical basics for recording and reconstructing processes in digital holography; the spectral properties and sampling requirements of the convolution kernel are discussed and the problem of spatial bandwidth adaptation is highlighted; Section 3 discusses three ways to adapt the spatial bandwidth of the convolution kernel to that of the object, either by using zero-padding, spectral scanning or adjustable magnification. Section 4 provides experimental results, so as to illustrate the algorithm principles. Section 5 draws the conclusions of the study.

1. Theoretical basics

1.1. Hologram recording

Let us consider the interference between a smooth-plane reference wave and a diffracted object wave. In the recording plane, the hologram is expressed as :

where $R(x', y') = a_R exp[-2i\pi(u_o x' + v_0 y')]$ is the reference plane wave at the recording plane, with spatial frequency $\{u_0, v_0\}$, and O is the wave diffracted in the recording plane by the object located at the distance d_0 from this plane. The object wave at the recording plane is given by a convolution formula (* means convolution) :

where $A(x, y) = A_0(x, y)\exp[i\psi_0(x, y)]$ is the object wave front at the object plane and $h(x, y, d_0)$ is the impulse response of free space propagation along distance d_0 . According to Goodman, we have [32 [Introduction to Fourier Optics]]:

We suppose that the digital hologram expressed in Eq. (1) is sampled by $M \times N$ data points corresponding to the useful number of pixels of the recording sensor.

1.2. Hologram reconstruction

There are mainly two ways to perform the numerical reconstruction of digitally recorded holograms. These methods are based on Eq. (2) and its possible different interpretations. At any reconstruction distance d_r, which may be different from d_0, the numerically-reconstructed hologram corresponds to the discrete version of the following equation:

Eq. (4) can be interpreted as the exact convolution formula as given in Eq. (3). It can also be interpreted as the two-dimensional discrete Fresnel transform, in which Eq.(3) now has a linear phase according to the approximation $(1+a)^{1/2} \approx 1 + a/2$ (with $a \ll 1$, i.e. $d_0 \gg \max(x^2 + y^2)$). The last way to calculate Eq. (4) consists in using the convolution theorem: in this case, the reconstructed object can also be written as follows (FT means Fourier Transform):

or

Eqs. (5) and (6) are two other possibilities to perform the reconstruction of the object in the spectral domain. Eq. (5) uses the transfer function of the free space propagation, which is the Fourier transform of the impulse response (exact or Fresnel, considering Eq. (3) and its linearized version). Eq. (6) uses the angular spectrum transfer function which is derived from the Helmholtz equation, by considering the object wave as the superposition of plane wavelets [32 [Introduction to Fourier Optics]]. This transfer function is analytically defined in the spatial frequency domain (u, v) as:

Note that G can also be simplified according to the Fresnel approximations by expanding the square root in the complex exponential to the first order, as for Eq. (3).

1.3. Spatial frequency spectrum of the hologram

Compared to classical image processing, one unusual aspect of digital holography is the localization property of the Fourier spectrum of the hologram, in regard to the physical object space. Let us consider the Fresnel transform of the hologram, calculated at any distance d_r. The reconstructed field is usually related to the Fresnel transform of the recorded hologram according to the following relation:

Considering that $\{u, v\} = \{x/\lambda d_r, y/\lambda d_r\}$ and that d_r tends towards infinity, then,

Eq. (9) means that the Fourier transform of the digital hologram is proportional to the reconstructed field at an infinite distance. The diffracted field at infinity is not focused $(d_r \neq \pm d_0,)$, so the object appears strongly blurred. However, its spatial distribution is similar to that of the spatial frequency spectrum. As a consequence, the digital hologram exhibits a singular property compared to classical Fourier analysis: the spatial frequency location in the Fourier spectrum corresponds to a spatial location in the object field (this point will be illustrated with Figure 2 in subsection 4.1). So, any spatial location in the object plane, given by $\{x_i, y_i\}$, corresponds to a spatial frequency location $\{u_i, v_i\} = \{x_i/\lambda d_r, y_i/\lambda d_r\}$. Note also that the center of the useful $+1$ order is localized at the spatial frequencies of the reference wave, i.e. $\{u_0, v_0\}$. Explications of this can be found in [29 [General theoretical formulation of image formation in digital Fresnel holography]].

1.4. Sampling requirements for the convolution formula using impulse response

In order to reconstruct the encoded object, the analytical functions of the previous sub-sections require to be spatially (versions of h) or spectrally (versions of G) sampled. The analysis of the sampling requirements is related to the oscillation properties of both functions. Note that h can be written as a complex oscillating function $h = a_h \exp(i\Theta_h)$ and that G is a pure oscillating complex function as $G = \exp(i\Theta_G)$. The local spatial frequencies of h are then given by (considering only the oscillating part of h) :

Furthermore, the spatial extents of h are related to the number of sampling points of the horizon on which h is defined and given by $[-x_{max}, +x_{max}]$ (resp.$[-x_{max}, +x_{max}]$) , with $x_{max} = Lp_x/2$ (resp. $y_{max} = Kp_y/2$) and (K, L) the number of sampling data points, (p_x, p_y) the pixel pitches of the recording plane. So, the useful bandwidth of the transfer function associated to h is simply:

According to Eq. (11), the spatial bandwidth decreases when the reconstruction distance increases and the spatial bandwidth is only adapted to reconstruct an object zone sized $Kp_y \times Lp_y$. In order to increase the reconstructed zone, by using Eq. (5), the spatial horizon, on which h is calculated, can be extended by increasing the values of K and L. This means that the spatial extent of the digital hologram must be also extended and then padded with zeros to a size equal to $K \times L$ (i.e.$K, L \geq M, N$). The impulse response will be correctly sampled if the Shannon conditions are fulfilled, leading to [39, [Fast algorithms for free-space diffraction patterns calculation]40 [Diffraction transfer function and its calculation of classic diffraction formula]]:

For example, if $K = L = 2048$, $p_x = p_y = 4.65\mu m$and $\lambda = 0.62328\mu m$ then $d_r \geq 70$ mm and if $K = L = 512$, $p_x = p_y = 4.65\mu m$ then $d_r \geq 17.5$ mm.

Eq. (12) induces a reverse relationship, which states that the function $h(x, y, d_r)$ will be correctly sampled up to a number of data points defined as such:

1.5. Sampling requirements for the convolution formula using the angular transfer function

According to the same approach as for the impulse response, the local spatial periods associated to G are now given by (Fresnel approximation):

Now, the spatial frequency extents in the Fourier plane are related to $u_{max} = 1/2p_x$ and $v_{max} = 1/2p_y$, leading to the spatial width of the angular spectrum function:

The sampling of G in the spatial frequency plane must also fulfill the Shannon conditions. Furthermore, the FFT computation of the hologram spectrum on $K \times L$ data points sets the pitches $\delta u, \delta v)$ in the spatial frequency plane. Then, we have $(\delta u, \delta v) = (1/\Delta T_x, 1/\Delta T_y) \leq (p_x/\lambda d_r, p_y/\lambda d_r)$, leading to:

Thus, the transfer function G will be correctly sampled $over\ the\ full\ digital\ spectrum$ from $K \times L$ data points:

However, if one aims at correctly sampling G, *only over the useful spatial bandwidth of the object wave* (and *not* on the full spectrum), then the maximum local spatial periods will be defined in the Fresnel conditions by ($\Delta A_x = \Delta A_y$ along x and y directions respectively):

With these conditions, the spatial frequency sampling pitches of G will be $(\delta u, \delta v) \leq (1/2T_{ix}^{max}, 1/2T_{iy}^{max}) = (1/\Delta A_x, 1/\Delta A_y)$, and G will be correctly sampled on the object spectrum from $K \times L$ data points:

Relation (19) means that the larger the object is, the harder the calculation by convolution is. Indeed, the number of data points must be at least equal to the ratio between the object size and the pixel pitch of the sensor. The next section discusses reconstruction convolution algorithms related to these sampling requirements.

2. Related reconstruction algorithms

2.1. Preliminary

The previous analysis of the sampling of the impulse response and of the transfer function showed that numerical reconstruction is not possible if the Shannon conditions are not fulfilled. The main problem is due to the spatial frequency bandwidth of the convolution kernel (impulse response or transfer function) that is not sufficient if the object is much more extended than the recording area. In the spatial frequency spectrum, a three-modal distribution is related to the three diffraction orders of Eq. (1), according to:

In Eq. (20), C_0 is the Fourier transform of the zero-order and C_1 is the Fourier transform of the $+1$ order. Figure 1(a) illustrates the spectral distribution in the Fourier plane. Note also that the transfer function of the convolution is a band-pass filter centered at $(0,0)$ spatial frequency, as illustrated in Figure 1(b). Thus, in order to reconstruct by convolution the virtual image localized at spatial frequencies (u_0, v_0), one needs to check the suitable frequency localization of the convolution kernel and the object-adapted spatial bandwidth. From Eq. (11), the spatial frequency extents of the object wave is:

So as to fully reconstruct the object, the spatial frequency extents of the convolution kernel must be at least that of the object, giving:

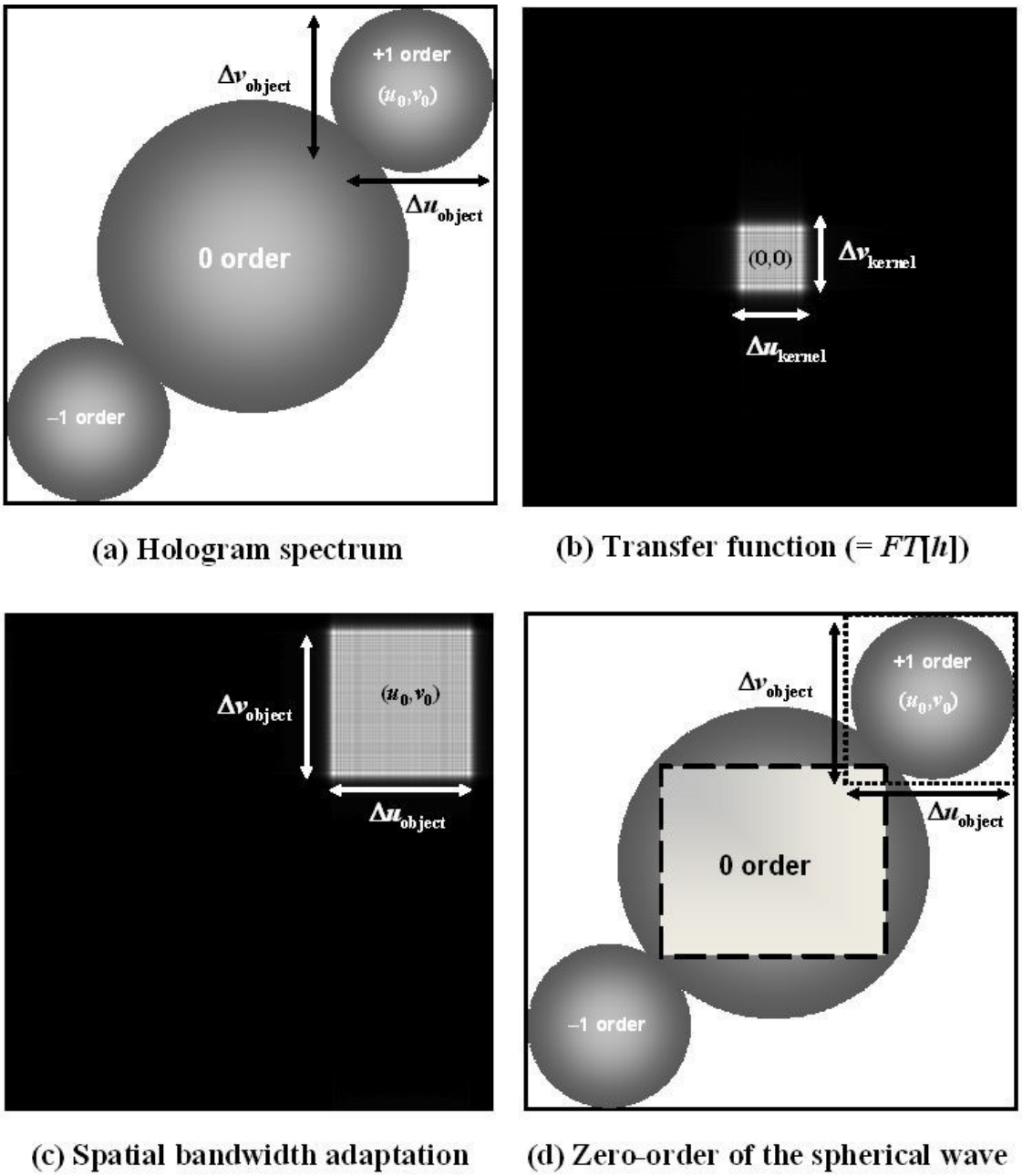

(a) Hologram spectrum (b) Transfer function (= $FT[h]$)

(c) Spatial bandwidth adaptation (d) Zero-order of the spherical wave

Figure 1. Hologram spectrum and adaptation of spatial bandwidth of the convolution kernel, a) hologram spectrum, b) Fourier transform of the impulse response, c) spatial frequency bandwidth adaptation, d) zero-order due to the spherical wave front

Figure 1(c) illustrates the adaptation of the spatial bandwidth of the kernel to that of the object.

The next sections propose three different strategies to increase the spatial frequency bandwidth of the convolution kernel. The first is based on the zero-padding of the impulse response or of the angular spectrum transfer function. The second is based on the design of a filter bank and consists in a spectral scanning of the object spectrum so as to recover the full bandwidth. The third consists in modifying the reconstruction distance so as to naturally increase the spatial bandwidth.

2.2. Zero-padding

From the previous section, a simple way to increase the spatial frequency bandwidth consists in using the zero-padding of the impulse response or the angular spectrum transfer function, to get:

leading to $\Delta A_x / p_x$. As pointed out with Eq. (19), the number of data points is the ratio between the object size and the pixel pitch of the sensor. So, the problem linked to the reconstruction of extended objects by using a convolution approach is tantamount to a problem of adaptation of the spatial frequency bandwidth. In order to reconstruct the hologram, the transfer function may be the Fourier transform of the impulse response (exact or Fresnel) or the angular spectrum transfer function (exact or Fresnel). For all these options, one must take into account the spectral localization and the spatial frequency extents of the bandwidth. The zero-padding of the digital hologram with $(K, L) > (M, N)$ leads to extending the horizon for the calculation of the impulse response of the free space propagation, or to an over-sampling of the angular transfer function. If the impulse response of free space propagation is used, the spectral localization can be obtained by using the modulation theorem. Centering at frequency $\{u_0, y_0\}$ is performed by spatially modulating h, according to:

If the angular spectrum transfer function is used, and as the transfer function must be a band-pass filter in the Fourier domain, one may limit the convolution kernel to the effective spectrum bandwidth and shift G in the spatial frequency space. From previous subsections, G must be bandwidth limited to satisfy sampling requirements. Thus, the associated transfer function is:

2.3. Filter bank

We have previously seen that zero-padding may extend the spatial frequency bandwidth. However, it is not sufficient since it leads to huge values for numbers K and L , when the object is extended compared to the sensor. A second approach consists in scanning the full object bandwidth with that of the convolution kernel. Let us suppose that we can calculate the reconstruction horizon on $L \times K$ data points. If the object size $\Delta A_x \times \Delta A_y$ is greater than $Lp_x \times Kp_y$, the number of scans in the x and y directions are respectively given by:

Thus, the reconstructed object will be obtained with the juxtaposition of $n_x \times n_y$ adjacent parcels. The full reconstructed object will then be sampled with $n_x L \times n_y K$ data points. In order to reconstruct an object parcel centered at $\{x_p, y_q\}$, $(p = [1, n_x]\,; q = [1, n_y])$, with a spatial extent of $\{Lp_x \times Kp_x\}$, the convolution kernel of spectral extents $(Lp_x / \lambda d_r) \times (Kp_y / \lambda d_r)$ must be centered at the spatial frequency $\{u_p, v_q\} = \{x_p / \lambda d_r, y_q / \lambda d_r\}$.
If the impulse response of free space propagation is used, the spectral localization at frequency $\{u_p, v_q\}$ can be obtained according to the modulation theorem as in Eq. (24):

From this, the associated transfer function is:

If the angular spectrum transfer function is used, the spectral localization and restriction are obtained by:

The useful set of spatial frequencies for the filter bank are given in x and y directions by $\{u_p, v_q\} = \{u_0 + k_x \frac{Lp_x}{\lambda d_r}, v_0 + k_y \frac{Kp_y}{\lambda d_r}\}$, with $k_x \epsilon \{-(n_x - 1)/2, +(n_x - 1)/2\}$ and $k_y \epsilon \{-(n_y - 1)/2, +(n_y - 1)/2\}$.

2.4. Adjustable magnification

The last method to extend the spatial frequency bandwidth is based on modifying the reconstruction distance. For a given value of $\{K, L\}$, if d_r decreases, then the spatial bandwidth of Eq. (23) increases. The modification of the reconstruction distance can be obtained by using a spherical reconstruction wave, instead of a plane wave. This means that in Eqs. (5) and (6) one needs to consider H multiplied by a spherical wave $w(x, y, R_c) = \exp(i\pi(x^2 + y^2)/\lambda R_c)$, with R_c its curvature radius. Note that several cases lead to the same effect. We have considered in subsection 2.1 the case of a plane reference wave to record the hologram. Here, we deal with the case of a recording plane wave (curvature radius $d_s = \infty$) and a numerical spherical reconstruction wave ($R_c \neq \infty$). The same effect could be obtained, first, by using a spherical recording wave ($d_S \neq \infty$) and a numerical plane reconstruction wave ($R_c = \infty$), second, by using a spherical recording wave ($d_s \neq \infty$) and a numerical spherical reconstruction wave ($R_c \neq \infty$). Note that the possibility of using a spherical reconstruction wave to adjust the magnification was also mentioned by Schnars et al in 2002 [41 [Digital recording and numerical reconstruction of holograms]]. However, they did not discuss any practical implementation.

At this stage, we need to consider the notion of "adjustable magnification" in digital holography. In classical holography, the concept of transverse magnification is perceptible since one can easily observe, before one's very eyes, the change in the size and position of the diffracted image if one modifies the laser wavelength or the curvature of the illuminating beam. However, with a numerical image, this notion is even less obvious. The notion of magnification is related to the observation horizon (sized $Lp_x \times Kp_y$) that is reconstructed by the numerical process. The reconstruction of an extended object, whose physical size $\Delta A_x \times \Delta A_y$ is larger than the horizon, is expected. So that the object may fully appear in the numerical field of view, a transversal magnification $\gamma = \min(Lp_x/\Delta A_x\ ; Kp_y/\Delta A_y)$ must be applied; this is the ratio between the horizon and the object widths. In this way, one may conceive that the adjustable magnification method results adjusting the reconstructed object size to that of the horizon, which is imposed by calculation capacities or computation speed.

Note that several authors proposed algorithms qualified "with adjustable magnification". In 2004, F. Zhang et al [42 [Algorithm for reconstruction of digital holograms with adjustable magnification,]] proposed an algorithm based on a double Fresnel transform resulting in the adjustment of the side length of the field of view. In 2010, J.F. Restrepo et al [43 [Magnified reconstruction of digitally recorded holograms by Fresnel-Bluestein transform]] discussed the adjustable magnification using the Fresnel-Bluestein transform. Both methods are based on the Fresnel transform (single or double) and the notion of magnification is linked to the ratio between the reconstructed pixel pitch and that of the sensor

According to the physical process which leads to holographic image reconstructions, the curvatures and distances are closely linked by this equation [32];

The transverse magnification is related to the ratio between reconstruction and recording distances:

Eq. (30) shows that the focus on the virtual image is not obtained for $d_r = -d_0$, but for a different distance that depends on the curvature of the recording reference wave and numerical reconstruction wave. Thus, this draws the basics of reconstruction with adjustable magnification: a spherical wave, either a reference or a reconstruction wave, will modify the reconstruction distance, which will modify the spatial frequency bandwidth of convolution, then leading to an adaptation to the object bandwidth. This can be quickly explained by Eq. (32):

The consequence is that the reconstructed object gets a size which is now compatible with that of the reconstruction horizon.

Note that $w(x, y, R_c)$ is also an oscillating function whose spatial bandwidth is localized at $(0,0)$ frequency with a spectral extent defined by :

Thus, the zero-order diffraction of the digital hologram will be superposed to a rectangular pattern sized $\lambda u_w \times \lambda v_w$. The more γ decreases, the more R_c decreases, the more the rectangular pattern and the convolution kernel increase. The transverse magnification must be optimized not to have overlapping between the spatial bandwidth of convolution and the rectangular pattern. Figure 1(d) illustrates the configuration in which the magnification leads to a rectangular pattern slightly overlapping the useful $+1$ order.

Depending on the magnification, the filtering of the object spectrum may include a part of this pattern, leading to undesirable spatial frequencies that will generate a parasitic spot in the field of view of the reconstructed object. In order to avoid such overlapping, the following condition must be verified:

Taking into account that $R_c = \gamma d_0(\gamma - 1)$ (case $d_s = \infty, R_c \neq \infty$), $0 < \gamma < 1$ (since the object is much larger than the recording area), $|\gamma - 1| = 1 - \gamma$, Eq. (34) becomes:

Given Eq. (33), the transversal magnification must be included in the interval defined by Eq. (36):

As regards the method based on the filter bank, the transfer function can be either the Fourier transform of the impulse response (exact or Fresnel) or the angular spectrum transfer function (exact or Fresnel). For all these options, one must take into account the spectral localization and the spatial frequency extents of the bandwidth. Since the transfer function is a band-pass filter in the Fourier domain, one may restrict it to the contour of the object and limit the convolution kernel to the effective object spectrum.

Thus, if the object is included in a circular zone ($\Delta A_x = \Delta A_y = \Delta A$), the impulse response can be chosen to be:

Similarly, the impulse response can be also defined for a rectangular object zone. This restriction of the spatial bandwidth leads to a convolution kernel perfectly adjusted to the object bandwidth. If the angular spectrum transfer function is used, the associated transfer function is thus (circular object):

The use of the adjustable magnification induces a modification in the spatial resolution of the reconstruction process. Since the reconstruction distance changes due to the magnification, the spatial resolutions are:

where ρ_x and ρ_y are the intrinsic spatial resolutions of the holographic process given by the spatial extents of the recording area [29 [General theoretical formulation of image formation in digital Fresnel holography]]. From Eq. (39) the spatial resolution is proportional to the magnification. Since $|\gamma| < 1$ (object larger than sensor), this would mean that the spatial resolution is increased by the process. This is of course not physically possible because the

numerical process can not easily transcend the fundamental limits. As indicated previously, the reconstruction process based on adjustable magnification consists in modifying the object size in the direct space so that it can "enter" the window of the reconstruction horizon. Thus, it is interesting to note that the ratio between the object size and the spatial resolution remains unchanged, either in the direct space or in the reconstructed space. This means that the resolution is not increased in the magnified object. The only effect of the algorithm is on the image "definition", similarly to the effect of zero-padding in the Fresnel transform [29 [General theoretical formulation of image formation in digital Fresnel holography],44, [Controlling image size as a function of distance and wavelength in Fresnel-transform reconstruction of digital holograms]45 [Pixel resolution control in numerical reconstruction of digital holography]].

3. Experimental demonstration

3.1. Zero-padding

Let us consider the numerical reconstruction of the digital hologram of a 1 coin (sized $\Delta A_x = \Delta A_y = \Delta A = 23.5mm$) that was recorded in a Fresnel configuration with $d_0 = 670mm, \lambda = 532nm, M = 1024, N = 1360$ and $p_x = p_y = 4.65\mu m$. The reference wave is adjusted to spatial frequencies $\{u_0, v_0\} = \{-71.01, -71.78\}mm^{-1}$. In this subsection, $d_r = -d_0$. The spatial frequency bandwidth of the object wave is then $\Delta u_{object} \times \Delta v_{object} = 65.95 \times 65.92mm^{-2}$. Given Eq. (19), one needs at least 5054×5054 data points to reconstruct the full object, which is greater than the calculation capacity of standard PC computers.

Figure 2(a) shows the reconstructed field obtained using the discrete Fresnel transform with $K = L = 2048$ data points. Figure 2(b) shows the spatial frequency spectrum of the digital hologram, exhibiting the three diffraction orders and the useful object spectral bandwidth.

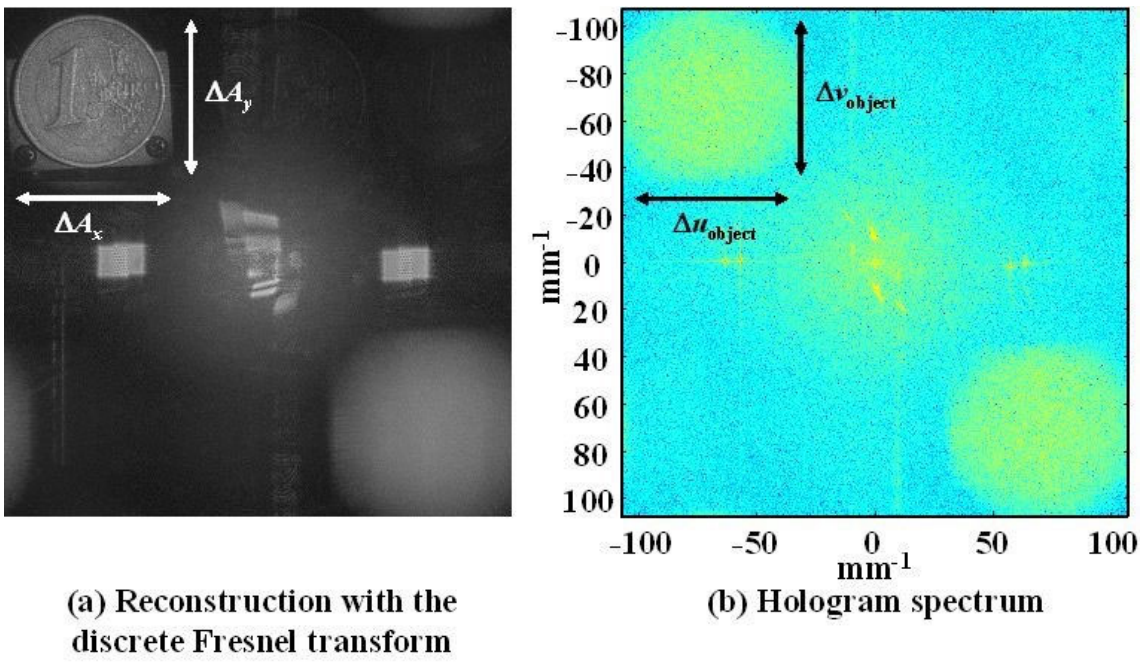

Figure 2. Discrete Fresnel transform (a) and experimental spatial frequency spectrum (b)

Figures 3(a),(b) show the transfer functions associated to the impulse response (exact) and angular spectrum transfer function (exact) when reconstructing with $K = 1024$ and $L = 1360$ (no zero-padding). The reconstructed area is then sized $4.76mm \times 6.32mm$, which corresponds to the physical size of the sensor. Figures 3(c),(d) show the reconstructed areas using the

transfer functions of Figures 3(a),(b): only the centre of the object can be obtained because of the narrowness of the spectral bandwidth of the kernel, which is only $\Delta u_{kernel} \times \Delta v_{kernel} = 17.41 \times 13.35 mm^{-2}$. Note that the transfer functions are both localized at the mean spatial frequency of the digital hologram and that their extents have a rectangular shape, similarly to the reconstruction horizon (Eqs. (24), (25)). With zero-padding, the reconstructed area can be extended until the computation limits of the computer. The computer used to reconstruct the hologram presented in this course was not able to reconstruct the object with 5054×5054 data points. When choosing $K = 1024$ and $L = 5000$, zero-padding is effective along the x direction, the reconstructed area is rectangular and sized $4.76mm \times 23.25mm$. So the reconstructed area included the full object width in the x direction. Similarly, choosing $K = 5000$ and $L = 1024$ leads to a vertical rectangular reconstructed zone.

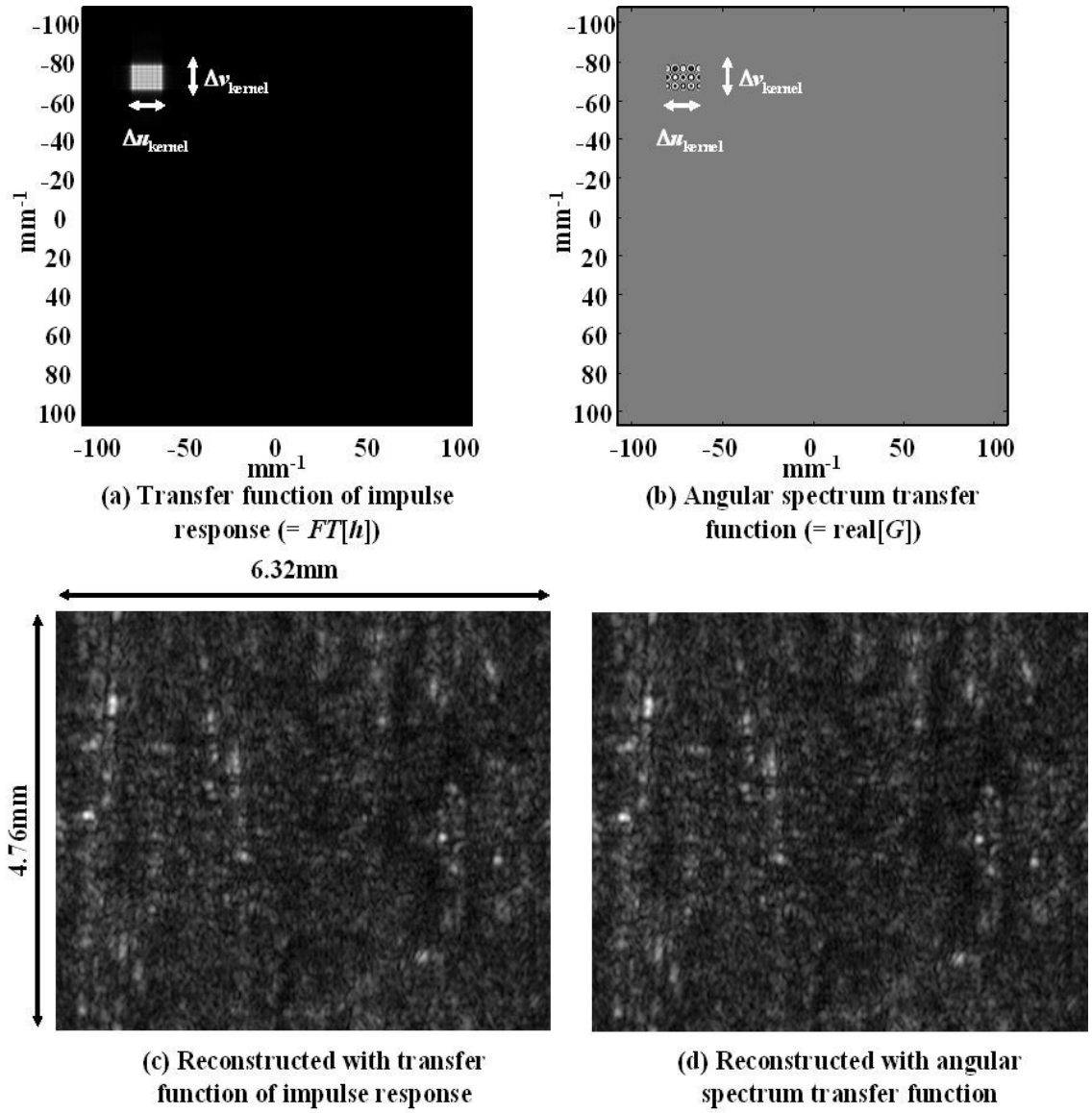

Figure 3. Reconstruction with convolution, a) Fourier transform of impulse response, b) angular spectrum transfer function, c) object zone reconstructed with impulse response, d) object zone reconstructed with angular spectrum transfer function

So as to illustrate these two cases, Figure 4 exhibits the transfer functions and the reconstructed object regions. Figures 4(a)(b) correspond respectively to horizontal and vertical rectangular areas for the transfer functions of the impulse response (a) and the angular spectrum transfer function (b). Figures 4(c), (d) show the rectangular regions corresponding to these transfer functions.

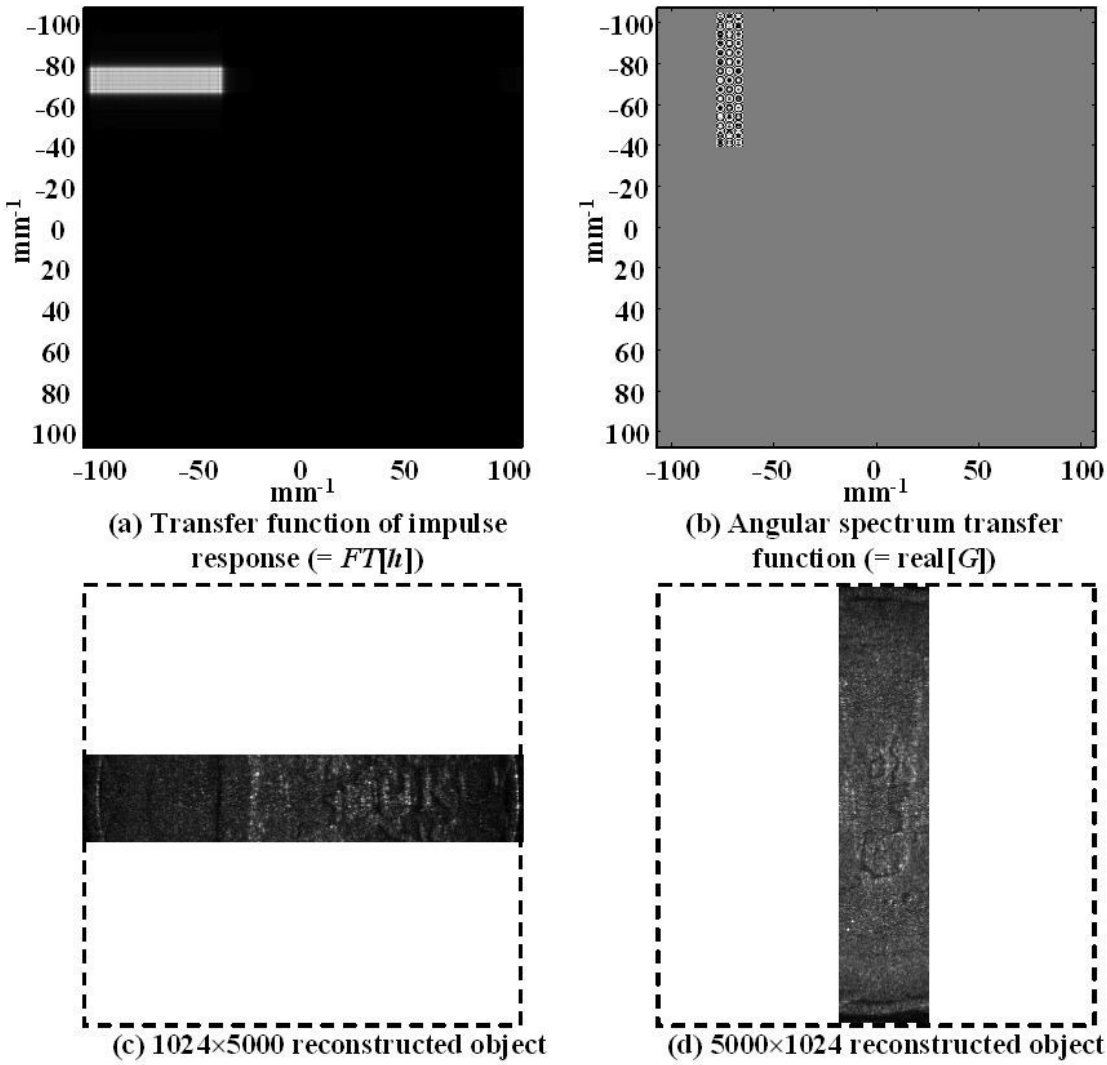

Figure 4. Anisotropic reconstruction with convolution, a) Fourier transform of impulse response, b) angular spectrum transfer function, c) object zone reconstructed with impulse response, d) object zone reconstructed with angular spectrum transfer function

Note that the reconstruction with convolution is equivalent to that given by the discrete Fresnel transform, but with an over-sampling of the calculated object. A convolution reconstruction with 5054×5054 data points is equivalent to a reconstruction with the Fresnel transform calculated over 16384×16384 data points.

As can be seen, the shape of the reconstructed zone can be freely chosen in the reconstructing process. However, such an approach is limited to a small amount of data points. The next section illustrates the case of reconstruction with the filter bank.

3.2. Filter bank scanning

In this subsection, $d_r = -d_0$. Choosing a reconstruction horizon sized $K \times L = 2048 \times 2048$ data points leads to $n_x \times n_y = 3 \times 3$ scans of the object spectrum. Then, the full reconstructed object will be sampled with 6144×6144 data points. This illustration uses the angular spectrum transfer function. The spectral bandwidth of the transfer function is $\Delta u_{kernel} \times \Delta v_{kernel} = 26.71 \times 26.71 mm^{-2}$ according to subsection 3.3.

Table 1 gives the spatial frequencies $\{u_p, v_q\}$ of the center of each filter used in the scanning process

Table 1. Values of the spatial frequencies for the filter bank

(p,q)	Spatial frequencies u_p (mm^{-1})	Spatial frequencies v_q (mm^{-1})
(1,1)	–97.72	–98.50
(1,2)	–97.72	–71.78
(1,3)	–97.72	–45.07
(2,1)	–71.00	–98.50
(2,2)	–71.00	–71.78
(2,3)	–71.00	–45.07
(3,1)	–44.28	–98.50
(3,2)	–44.28	–71.78
(3,3)	–44.28	–45.07

Table 1. Values of the spatial frequencies for the filter bank

Figure 5 illustrates the principle of the reconstruction. The full object is obtained after juxtaposing the different adjacent regions calculated with each filter of the spectrum scan.

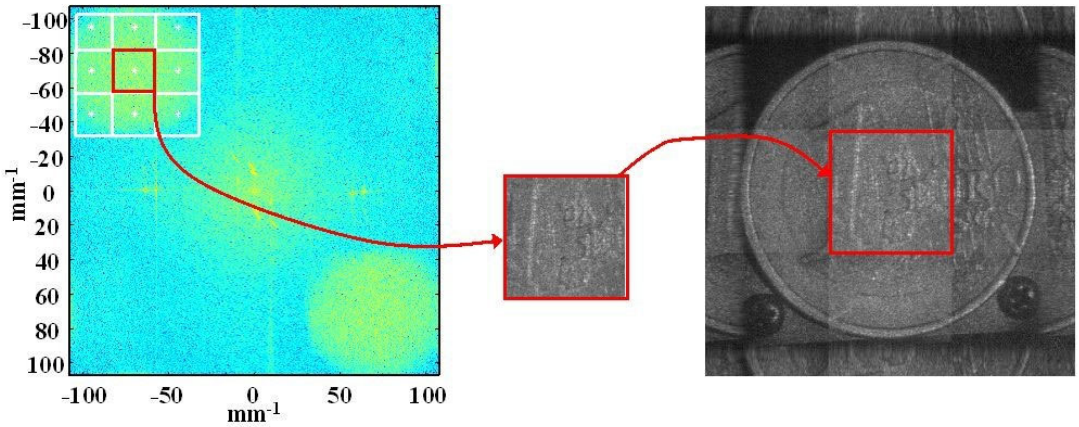

Figure 5. Principle of the spectrum scanning algorithm, a) hologram spectrum paving (white square line), b) parcel obtained with the central filter, c) full-field object reconstructed with adjacent parcels

Figure 6(a) shows the full object obtained using the transfer function of the impulse response, whereas Figure 6(b) shows the one obtained with the angular spectrum transfer function. Note that the images obtained with the scanning process do not have a top quality. Indeed, aliasing effects contribute to decreasing the image quality. Figure 6(c) identifies the aliasing regions and their corresponding zones in the object image (rectangles with the same color). Aliasing is likely caused by a non-consistency in the sampling process.

Sections 2.4 and 2.5 discussed the sampling conditions for both the impulse response and the angular spectrum. These conditions are satisfied in the filter bank. However, these conditions do not take into account the edge effects that lead to extend the spatial bandwidth in the

Fourier plane; or that virtually lead to extend the reconstructed object zone in the reconstructed plane.

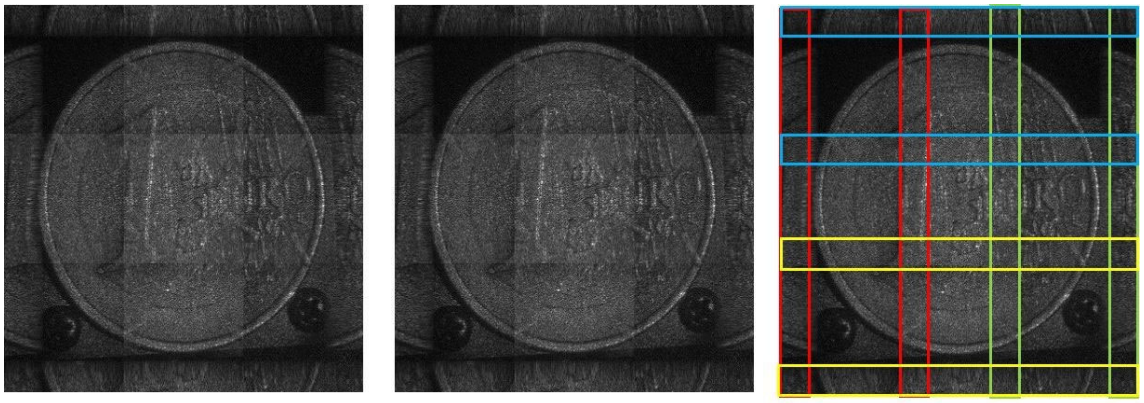

(a) Full object reconstructed with transfer function of impulse response

(b) Full object reconstructed with angular spectrum transfer function

(c) Identification of aliasing zones

Figure 6. Reconstructed object using the spectrum scanning, a) with the impulse response, b) with the angular spectrum, c) highlight of the edge effects leading to aliasing

So as to clarify this purpose, Figure 7(a) shows the profiles of the three adjacent filters obtained with the Fourier transform of the impulse response. The dashed line indicates the zone effectively reconstructed by the convolution kernel localized at the center of the bank. Edge effects can be observed and they contribute to about to the enlarging of the bandwidth of the kernel. Thus, for a region with L data points, about $L/2$ data points will be overlapped. The solution to this problem is to set an overlapping of the spectral bandwidth of the filter bank as illustrated in Figure 7(b). So, one needs to pave the spectrum with $((2n_x - 1) \times (2n_y - 1)$ scans. In Figure 7(b) each rectangular dashed line corresponds to the reconstructed zone ($L/2$ data points) that will be used for the adjacent parcels of each reconstructed horizon (L data points).

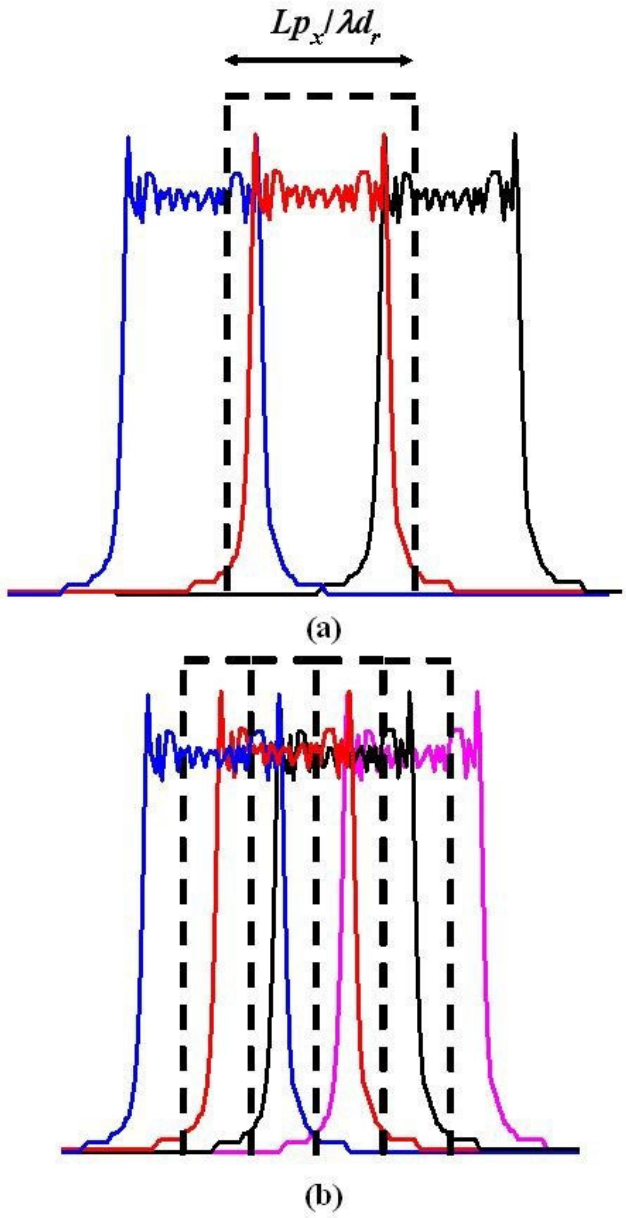

Figure 7. Overlapping of transfer functions of the filter bank, a) profiles of three adjacent filters, b) overlapping of the spectral bandwidth of the filter bank

For the 1 coin, one can choose $K \times L = 2048 \times 2048$ and keep only $M \times N = 1024 \times 1360$ data points in each parcel. So, the number of scans is $5 \times 4 = 20$ and the full object is now sampled with 5440×5120 data points. Figures 8(a), (b) show the reconstructed objects obtained with this procedure. The image quality is substantially increased. A slight overlapping in the x direction remains, but the overlapping has completely disappeared in the y direction. Indeed, choosing to keep 1024 data points is in agreement with the condition stated previously. Thus, one should keep 1024×1024 data points and $5 \times 5 = 25$ scans to completely avoid the aliasing in both directions. Of course, such a procedure increases the number of scans and requires allocating a higher memory capacity to the computer. Furthermore, the reconstruction process is longer. The next section illustrates how to reduce the computation time and get an effective full-field object reconstruction by using the convolution with adjustable magnification.

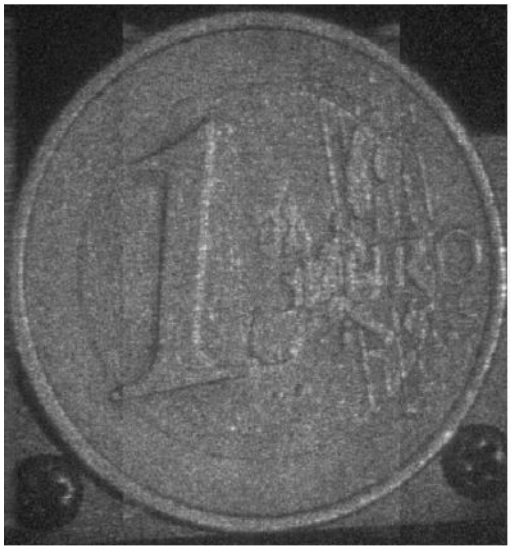

(a) Full object reconstructed with transfer function of impulse response (50% overlapping)

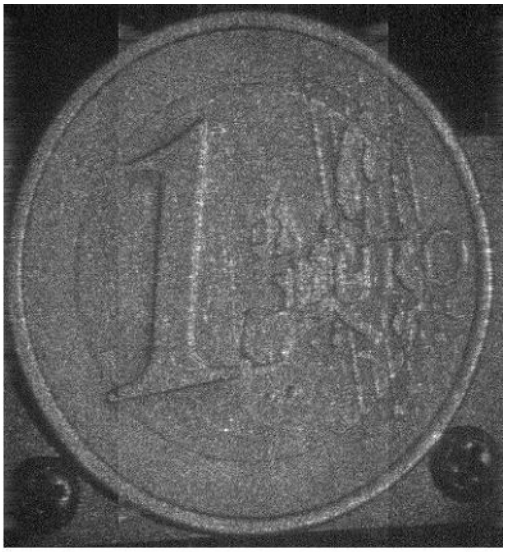

(b) Full object reconstructed with angular spectrum transfer function (50% overlapping)

Figure 8. Full object reconstructed with overlapping of the transfer functions, a) object zone reconstructed with impulse response, b) object zone reconstructed with angular spectrum transfer function

3.3. Adjustable magnification

Choosing a reconstruction horizon sized $K \times L = 2048 \times 2048$ data points leads to a reconstructed area sized $Kp_y \times Lp_x = 9.52mm \times 9,52mm$. For a given magnification, Eqs. (30) and (31) give the reconstruction distance and the curvature radius of the numerical spherical wave. Table 2 gives the parameters and Figure 9 shows the reconstruction process for different values of γ. The transfer function is that of the angular spectrum (exact).

Table 2. Values of the reconstruction parameters for K=L=2048 data points

γ	d_r (mm)	R_c (mm)
1	−670	∞
0.6	−402	−1005.00
0.4	−268	−446.67
0.3	−201	−287.14
0.25	−167.5	−223.33
0.1	−67	−74.44

Table 2. Values of the reconstruction parameters for K=L=2048 data points

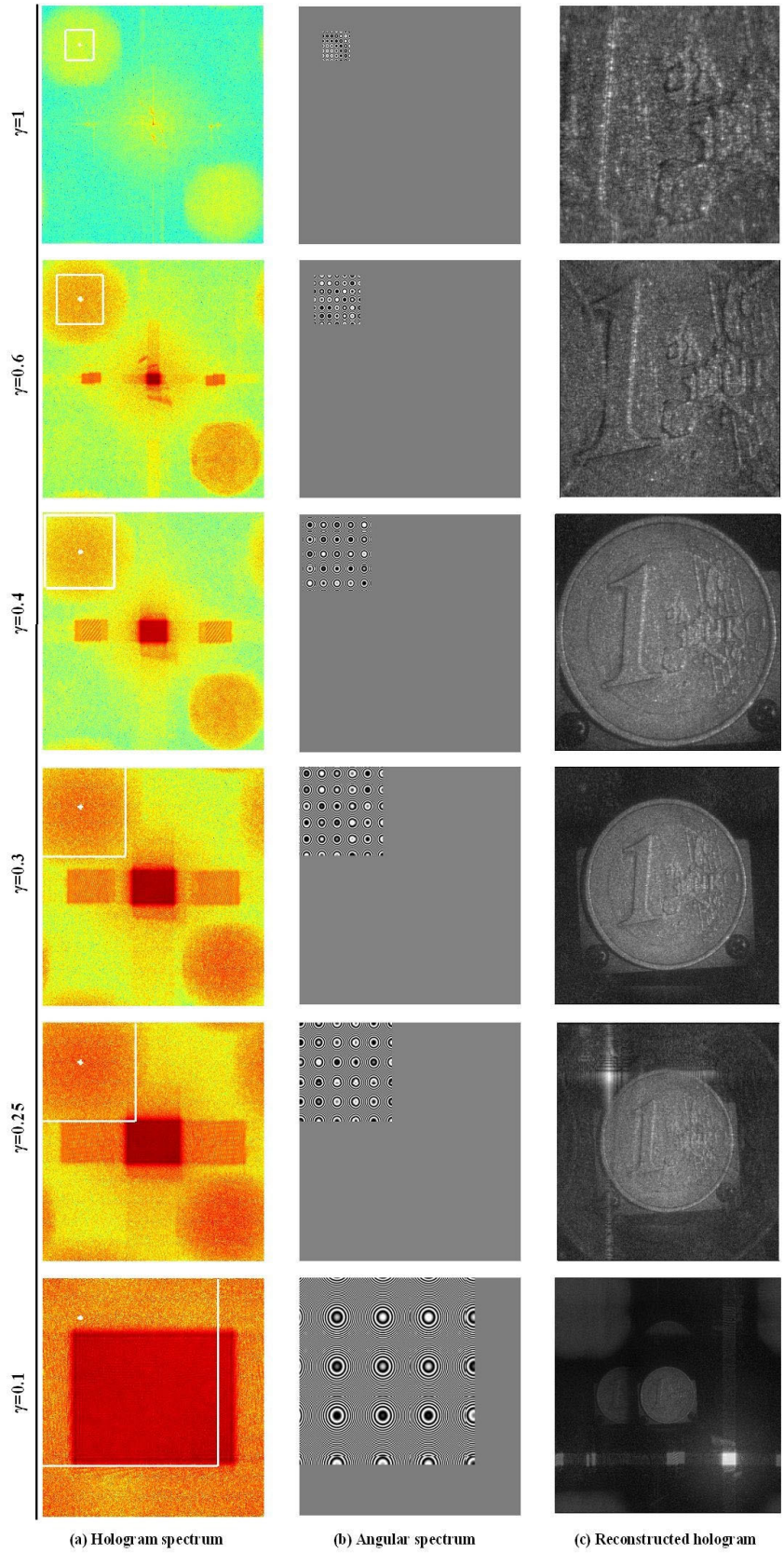

Figure 9. Reconstructions with adjustable magnification, a) hologram spectrum and spatial bandwidth limits, b) angular spectrum transfer function, c) reconstructed object

The case with $\gamma = 1$ corresponds to the classical convolution in which the reconstruction wave is a plane wave. In this configuration, only the centre of the object if reconstructed (see

Figures 3(c),(d)). The more the γ magnification is decreased, the more the reconstructed zone is extended. The reader may bear in mind that the size of the reconstructed zone is kept constant whatever the value of γ and that the process simply authorizes the modification of the object size in the direct space. From $\gamma = 0.405 = \min(Lp_x/\lambda A_x, Kp_y/\lambda A_y)$, one can see the full object appear in the field of view. Note that the more γ is decreased, the more the rectangular area of the zero order is increased. With the above mentioned parameters, Eq. (36) leads to $0.278 < \gamma < 0.405$. Thus, for $\gamma = 0.25 < 0.278$, the rectangular area is overlapping the useful spectral bandwidth of the convolution kernel.

The consequence is that unwanted parasitic spots appear in the field of view and contribute to degrading the image quality. Furthermore, from a certain value of γ, the condition of Eq. (12) is not fulfilled for the curvature radius R_c : spectral aliasing appears and leads to replica in the field of view as it is the case for $\gamma = 0.1$. Contrary to the method of spectral scanning, the computation time does not depend on the object size but solely on the size of the reconstruction horizon.

3.4. Summary

The different approaches were compared through the computation time required to reconstruct the 1 coin. The computer includes a Pentium Intel Core 2 CPU at 2.33GHz and RAM at 2Go. The software is developed with Matlab. Figure 10 shows the reconstruction time versus the algorithm. The reconstructed image is also shown. The discrete Fresnel transform is the most rapid computation but it is not a convolution method, since the sampling pixel pitch depends on distance and wavelength. The method using the adjustable magnification gives the best compromise between rapidity and efficiency to reconstruct large objects.

Reconstruction method	Computation time (s)	Number of sampling points in reconstructed object	Reconstructed image
Fresnel Transform with zero-padding to 2048×2048	4.719	629×629	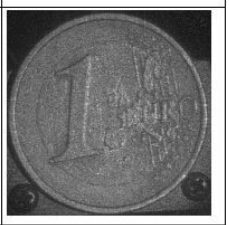
Convolution with zero-padding	out of memory	5000×5000	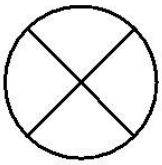
Adjustable magnification with angular spectrum	7.18	2048×2048	
Adjustable magnification with impulse response	11.57	2048×2048	
Filter banc with angular spectrum	94.96	5120×5440	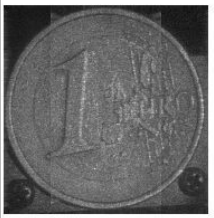
Filter banc with impulse response	158.84	5120×5440	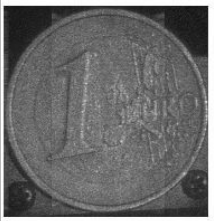

Figure 10. Comparison of the reconstruction algorithms

* *
*

The course has presented three different approaches to reconstruct a digital hologram using a convolution method. A basic discussion about the sampling requirements has highlighted the strong constraints to reconstruct extended objects with convolution, especially concerning spectral aliasing. The discussion was developed on the basis of both the angular spectrum transfer function and the impulse response of free space propagation. Both lead to bandwidth limited transfer functions and a size-reduced field of view. It was established that the problem of convolution is due to a limited spatial frequency bandwidth. Thanks to the increase of this bandwidth, extended objects can be reconstructed. As a result, the number of required data points is given by the ratio between the object size and the pixel pitch.

The first approach deals with the zero-padding of the digital hologram and exhibits limitation due to the increase in the number of data points. Depending on the object size and computation capacities, it may be impossible to reconstruct an extended object. The second approach is based on the joint property of the space-frequency localization of a digital hologram and its reconstructed field. Such a property is easily demonstrated through the Fresnel transform. With this method, the local images are used to reconstruct the full object by parceling the field of view. The number of parcels, and thus the number of spectral scans, depends on the ratio between the object size and the chosen reconstruction horizon. Furthermore, the computation time depends on the number of scans that must be performed. The problem of spectral aliasing, which leads to edge effects, has been addressed with an increase of the number of scans and thus of the computation time. This approach was developed on the basis of both the angular spectrum transfer function and the impulse response of free space propagation. The third approach uses the concept of adjustable magnification. It is based on the use of a numerical spherical reconstruction wave front whose curvature radius induces a change in the reconstruction distance and thus an increase of the spatial bandwidth of convolution. The reconstruction of the object is single shot and the computation time is strongly reduced compared to the spectral scanning algorithm. As a consequence, the adjustable magnification is quite useful to reconstruct digital color holograms encoding extended objects since the reconstruction horizon does not depend on the wavelengths.

Bibliographie

[Algorithm for reconstruction of digital holograms with adjustable magnification,] F. Zhang, I. Yamaguchi, L. P. Yaroslavsky, ‘‘Algorithm for reconstruction of digital holograms with adjustable magnification," *Optics Letters*, Vol. 29, 1668-1670 (2004).

[Color lensless digital holographic microscopy with micrometer resolution] J. Garcia-Sucerquia, “Color lensless digital holographic microscopy with micrometer resolution,” *Optics Letters*, Vol. 37, N°10, 1724-1726 (2012).

[Complex-wave retrieval from a single off-axis hologram] M. Liebling, T. Blun, M. Unser, “Complex-wave retrieval from a single off-axis hologram,” *J. Opt. Soc. Am. A*, Vol. 21, 367-377 (2004).

[Controlling image size as a function of distance and wavelength in Fresnel-transform reconstruction of digital holograms] P. Ferraro, S. De Nicola, G. Coppola, A. Finizio, D. Alfieri, G. Pierattini, “Controlling image size as a function of distance and wavelength in Fresnel-transform reconstruction of digital holograms”, *Optics Letters*, Vol. 29, N°8 (2004).

[Diffraction from a wavelet point of view] L. Onural, “Diffraction from a wavelet point of view,” *Optics Letters*, Vol. 18, 846-848 (1993).

[Diffraction transfer function and its calculation of classic diffraction formula] J.C. Li, Z. Peng, Y. Fu, ‘‘Diffraction transfer function and its calculation of classic diffraction formula”, *Optics Communications*, Vol. 280, 243-248 (2007).

[Digital in-line holographic microscopy] J. Garcia-Sucerquia, W. Xu, S. Jericho, P. Klages, M. Jericho, H.J. Kreuzer, “Digital in-line holographic microscopy,”, *Applied Optics*, Vol. 45, N°5, 836-850 (2006).

[Digital recording and numerical reconstruction of holograms] U. Schnars, W. Jüptner, ‘‘Digital recording and numerical reconstruction of holograms," *Measurement Science and Technology*, Vol. 13, R85-R101 (2002).

[Digital recording and numerical reconstruction of lens less Fourier holograms in optical metrology] C. Wagner, S. Seebacher, W. Osten, W. Jüptner “Digital recording and numerical reconstruction of lens less Fourier holograms in optical metrology,” *Applied Optics*, Vol. 38, 4812-4820 (1999).

[Digital three-color holographic interferometry for flow analysis] J. M. Desse, P. Picart, P. Tankam, “Digital three-color holographic interferometry for flow analysis”, *Optics Express*, Vol. 16, 5471-5480 (2008).

[Direct recording of holograms by a CCD target and numerical reconstruction] U. Schnars, W. Jüptner, ‘‘Direct recording of holograms by a CCD target and numerical reconstruction", *Applied Optics*, Vol. 33, 179-181 (1994).

[Direct shape measurement by digital wave front reconstruction and multi-wavelength contouring] C. Wagner, W. Osten, S. Seebacher, “Direct shape measurement by digital wave front reconstruction and multi-wavelength contouring,” *Optical Engineering*, Vol. 39, N°1, 79-85 (2000).

[Dynamic digital holographic interferometry with three wavelengths] N. Demoli, D. Vukicevic, M. Torzynski, “Dynamic digital holographic interferometry with three wavelengths,” *Optics Express*, Vol. 11, 767-774 (2003).

[Effect of the fill factor of CCD pixels on digital holograms: comment on the paper] C.S. Guo, L. Zhang, Z.Y. Rong, H.T. Wang, “Effect of the fill factor of CCD pixels on digital holograms: comment on the paper,” *Optical Engineering* 42, 2768-2772 (2003).

[Fast algorithms for free-space diffraction patterns calculation] D. Mas, J. Garcia, C. Ferreira, L.M. Bernardo, F. Marinho, "Fast algorithms for free-space diffraction patterns calculation," *Optics Communications,* Vol. 164, 233-245 (1999).

[Frequency analysis of digital holography] Th. Kreis, "Frequency analysis of digital holography," *Optical Engineering*, Vol. 41, 771-778 (2002).

[Frequency analysis of digital holography with reconstruction by convolution] Th. Kreis, "Frequency analysis of digital holography with reconstruction by convolution," *Optical Engineering*, Vol. 41, 1829-1839 (2002).

[General theoretical formulation of image formation in digital Fresnel holography] P. Picart, J. Leval, "General theoretical formulation of image formation in digital Fresnel holography," *J. Opt. Soc. Am. A*, Vol. 25, 1744-1761 (2008).

[Image formation in phase shifting digital holography and application to microscopy] I. Yamaguchi, J. Kato, S. Ohta, J. Mizuno, "Image formation in phase shifting digital holography and application to microscopy," *Applied Optics*, Vol. 40, 6177-6186 (2001).

[Image reconstruction for in-line holography with the Yang-Gu algorithm] Y. Zhang, G. Pedrini, W. Osten, H.J. Tiziani, "Image reconstruction for in-line holography with the Yang-Gu algorithm," *Applied Optics*, Vol. 42, 6452-6457 (2003).

[Imaging analysis of digital holography] L. Xu, X. Peng, Z. Guo, J. Mia, A. Asundi, "Imaging analysis of digital holography", *Optics Express* 13, 2444-2452 (2005).

[Introduction to Fourier Optics] J.W. Goodman, *Introduction to Fourier Optics* (Second Edition, McGraw-Hill Editions, New York, 1996).

[Large step-height measurements using multiple-wavelength holographic interferometry with tunable laser diodes] A. Wada, M. Kato, Y. Ishii, "Large step-height measurements using multiple-wavelength holographic interferometry with tunable laser diodes," J*OSA A*, Vol. 25, N°12, 3013-3020 (2008).

[Magnified reconstruction of digitally recorded holograms by Fresnel-Bluestein transform] J. F. Restrepo, J. Garcia-Sucerquia, "Magnified reconstruction of digitally recorded holograms by Fresnel-Bluestein transform," *Applied Optics*, Vol. 49, 6430-6435 (2010).

[Method of digital holographic recording and reconstruction using a stacked color image sensor] P. Tankam, P. Picart, D. Mounier, J.M. Desse, J.C. Li, "Method of digital holographic recording and reconstruction using a stacked color image sensor," *Applied Optics*, Vol. 49, N°4, 320-328 (2010).

[Methods of digital holography: a comparison] Th. Kreis, M. Adams, W. Jüptner, "Methods of digital holography: a comparison," *Proc. SPIE* 3098, 224-233 (1997).

[Microscopic TV holography for MEMS deflection and 3-D surface profile characterization] U. P. Kumar, B. Bhaduri, N. K. Mohan, M. P. Kothiyal, A. K. Asundi, "Microscopic TV holography for MEMS deflection and 3-D surface profile characterization," *Optics and Lasers in Engineering*, Vol. 46, 687-694 (2008).

[Multiple-wavelength digital holographic interferometry using tunable laser diodes] A. Wada, M. Kato, Y. Ishii, "Multiple-wavelength digital holographic interferometry using tunable laser diodes," *Applied Optics*, Vol. 47, No. 12, pp. 2053-2060 (2008).

[Off-axis digital hologram reconstruction: some practical considerations] N. Verrier, M. Atlan, "Off-axis digital hologram reconstruction: some practical considerations," *Applied Optics*, Vol. 50, N°34, H136-H146 (2011).

[Parallel phase-shifting color digital holography using two phase shifts] T. Kakue, T. Tahara, K. Ito, Y. Shimozato, Y. Awatsuji, K. Nishio, S. Ura, T. Kubota, O. Matoba, "Parallel phase-shifting color digital holography using two phase shifts," *Applied Optics*, Vol. 48, N°34, H244-H250 (2009).

[Parallel phase-shifting digital holography capable of simultaneously capturing visible and invisible three-dimensional information] T. Kakue, K. Ito, Y. Awatsuji, K. Nishio, T. Kubota, O. Maoba, "Parallel phase-shifting digital holography capable of simultaneously capturing visible and invisible three-dimensional information," *Journal of Display Technology*, Vol.6, N°10, 472-478 (2010).

[Parallel two-step phase-shifting digital holography] Y. Awatsuji, T. Tahara, A. Kaneko, T. Koyama, K. Nishio, S. Ura, T. Kubota, O. Matoba, "Parallel two-step phase-shifting digital holography," *Applied Optics*, Vol. 47, N°19, D183-D189 (2008).

[Phase imaging of cells by simultaneous dual wavelength reflection digital holography] A. Khmaladze, M. Kim, C-M. Lo, "Phase imaging of cells by simultaneous dual wavelength reflection digital holography", *Optics Express*, Vol. 16, 10900-10911 (2008).

[Phase shifting color digital holography] I. Yamaguchi, T. Matsumura, J. Kato, "Phase shifting color digital holography," *Optics Letters*, Vol. 27, 1108-1110 (2002).

[Phase-shifting digital holography] I. Yamaguchi, T. Zhang, "Phase-shifting digital holography," *Optics Letters* 22, 1268-1270, (1997).

[Pixel resolution control in numerical reconstruction of digital holography] L. Yu, M. K. Kim, "Pixel resolution control in numerical reconstruction of digital holography", *Optics Letters*, Vol. 31, 897-899 (2006).

[Pulsed digital holography for high-speed contouring that uses a two-wavelength method] G. Pedrini, P.hilipp Fröning, Hans J. Tiziani and Mikhail E. Gusev, "Pulsed digital holography for high-speed contouring that uses a two-wavelength method," *Applied Optics*, Vol. 38, N°16, 3460-3467 (1999).

[Quantitative phase imaging by three-wavelength digital holography] C. J. Mann, P. R. Bingham, V. C. Paquit, K. W. Tobin, "Quantitative phase imaging by three-wavelength digital holography", *Optics Express*, Vol. 16, N° 13, 9753-9764 (2008).

[Real-time dual-wavelength digital holographic microscopy with a single hologram acquisition] J. Kuhn, T. Colomb, F. Montfort, F. Charriere, Y. Emery, E. Cuche, P. Marquet, C. Depeursinge, "Real-time dual-wavelength digital holographic microscopy with a single hologram acquisition," *Optics Express*, Vol. 15, 7231-7242 (2007).

[Real-time three-sensitivity measurements based on three-color digital Fresnel holographic interferometry] P. Tankam, Q. Song, M. Karray, J.C. Li, J.M. Desse, P. Picart, "Real-time three-sensitivity measurements based on three-color digital Fresnel holographic interferometry," *Optics Letters*, Vol. 35, N°12, 2055-2057 (2010).

[Reconstruction of in-line digital holograms from two intensity measurements] Y. Zhang, G. Pedrini, W. Osten, H.J. Tiziani, "Reconstruction of in-line digital holograms from two intensity measurements," Optics Letters 29, 1787-1789 (2004).

[Recording and reconstruction of a color holographic image by using digital lensless Fourier transform holography] J. Zhao, H. Jiang, J. Di, "Recording and reconstruction of a color holographic image by using digital lensless Fourier transform holography," *Optics Express*, Vol. 16, 2514-2519 (2008).

[Surface shape measurement by phase-shifting digital holography with a wavelength shift] I. Yamaguchi, T. Ida, M. Yokota, K. Yamashita, "Surface shape measurement by phase-shifting digital holography with a wavelength shift," *Applied Optics*, Vol. 45, N°29, 7610-7616 (2006).

[Use of digital color holography for crack investigation in electronic components] P. Tankam, P. Picart, "Use of digital color holography for crack investigation in electronic components," *Optics & Lasers in Engineering*, Vol. 49, N°11, 1335-1342 (2011).

[Wavelength-scanning digital interference holography for tomographic three-dimensional imaging by use of the angular spectrum method] L. Yu, M. K. Kim, "Wavelength-scanning digital interference holography for tomographic three-dimensional imaging by use of the angular spectrum method," *Optics Letters*, Vol. 30, 2092-2094 (2005).